

Reflected Wave Modeling Techniques for PWM AC Motor Drives

G. Skibinski R. Kerkman D. Leggate J. Pankau D. Schlegel

Rockwell Automation - Allen Bradley Standard Drives Division
6400 W. Enterprise Drive PO Box 760
Mequon, WI 53092 (414) - 512 - 7151 (414) - 512 - 8300 Fax

Abstract: Reflected wave transient voltages that are impressed on drive output cables and low voltage ac induction motors are simulated with an excitation source of steep fronted dv/dt pulse waveforms from a Pulse Width Modulated (PWM) voltage source inverter. Motivation for system simulation arises from a need to correlate reflected wave peak voltage and risetime with the dielectric insulation capability of both motor and cable. Simulations based on an accurate system model also allow investigation into the effects of changing wire gauge, motor hp, cable distance or addition of drive output filters. System parameters of the inverter, cable and motor model are investigated in detail. Special emphasis is given to the importance of modeling cable skin and proximity effects. Simulation, measured lab and field results are compared. The main objective of the paper is to propose a reflected wave building block model that uses existing software on the market, is simple, computationally fast, easily configurable, reasonably accurate and allows investigation with wide variation of system parameters.

I. Introduction

A. History of Transmission Line Models

Power systems have traditionally had a need to study voltage transients on utility equipment. Transient Network Analyzer's (TNA's) of the analogue computer type were developed in the late 1930's. More sophisticated analog - digital hybrid computers were seen in the early 1970's. The Electro Magnetic Transients Program (EMTP) emerged in the late 1970's [1] with a capability to simulate line to line and line to ground voltage transients for the PWM drive system shown in Fig. 1. The EMTP has a sophisticated multi-mode cable model that encompasses many cable constructions, but it is expensive and not user friendly. SPICE simulators [2] are inexpensive and have a lossless transmission line model that accurately predicts motor terminal voltages when drive output filters or motor termination filters are used, as in Fig. 2. In this case, filter characteristics rather than the lossless line model dominates the transient response. However, the lossless line assumption of SPICE is grossly inaccurate with the unterminated motor case of Fig. 3. A SPICE lumped parameter cable model may be used but this creates inaccuracies as discussed in Section IV-D. The lumped parameter cable model may be split into an equivalent distributed π model with the total line length separated into multiple distributed π equivalent sections. However,

this also creates inaccuracies in reflected wave modeling as discussed in Section IV-D. A distributed or equivalent π cable model in Fig. 1 has been used for reflected wave modeling. However, a more accurate, cable modeling technique that encompasses many cable construction types is proposed that uses a transmission line model with a transport delay function in Fig. 1 for inverter - cable- motor investigation.

The proposed simulator package is SIMULINK [3]. The transport delay feature of the program is used to simulate the traveling wave propagation time and line oscillation frequency (f_o) fairly accurately. Cable skin and proximity effects of cable resistance that are a function of f_o may also then be determined accurately. The step source function models the semiconductor risetime from the drive. The motor is modeled with a combination of motor surge impedance, resistance, capacitance and winding inductance. Advantages include low cost, fast simulation time and ability to change building blocks easily. Many of the system parameters are not readily known in published literature or are difficult to predict, so an investigation into model parameters for the three basic building blocks of drive, cable and motor is done. As with any simulation, model accuracy is only as good as the input data quality. However, it is shown that simulation and experimental results are within acceptable tolerances.

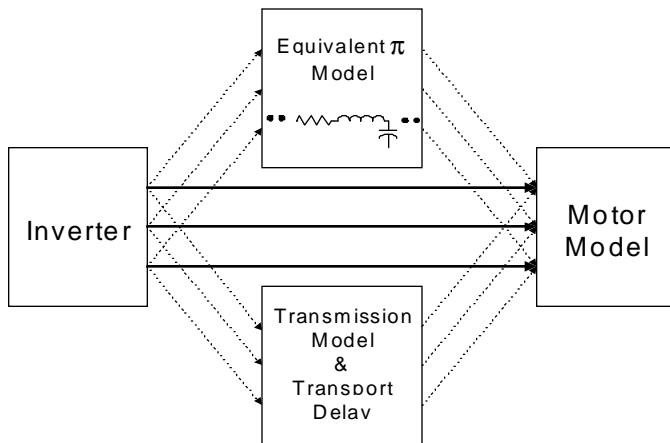


Figure 1 PWM Drive System Model

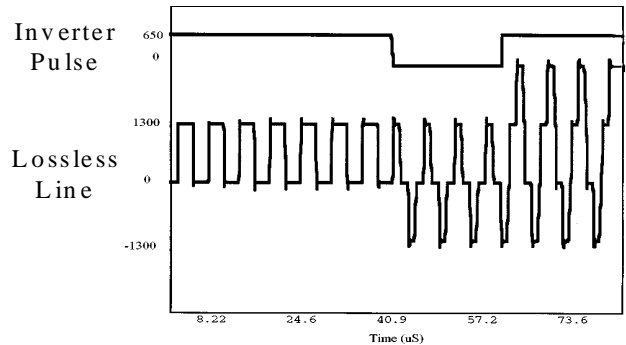


Figure 2 Inaccurate SPICE Simulation using Lossless Line and High Impedance Load at Receiving End.

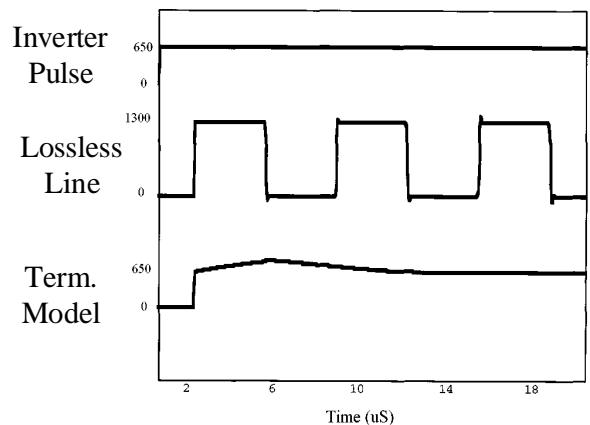


Figure 3 Accurate SPICE Simulation using Lossless Line and Termination Network at Receiving End.

II. System Model

Ac drive systems are complex and require simulations to aid their design. The complexity of a simulation is dictated by the particular subsystem analyzed. Evaluation of the effects of long cables and output filter devices on bearing currents and other high frequency effects necessitate simulation times based on the smallest eigenvalues.

A. Reduction of 3 Phase Circuit to 2 Wire Transmission Line

The basic 3 wire plus ground system of Fig. 1 may be reduced to a two wire transmission line model in SIMULINK, since the inverter sine triangle modulator only switches one device at a time. Thus, there is always two parallel legs in steady state with a return third single leg that is switched on. Cable and motor surge impedance parameters are also measured in this state. The goal of this simplified analysis is to simulate line to line voltage transients at the receiving end and does not take into account the cross coupling into the common mode circuit. Results are shown to agree with measured waveforms.

B. Block Diagram of System Model

Fig. 4 displays a SIMULINK block representation of an inverter drive system, with each subsystem - inverter (source), cable (transport delay), and machine (load) - expanded to show the respective component. The model is based on a distortionless line, transport delay process and lossy line assumptions [4]. Although lacking the effects of distortion, the model is adequate for preliminary investigation into over voltages. The forward and backward delay blocks keep track of the traveling wave by storing the forward (V_{fs}) and backward (V_{br}) voltages. The memory required is a function of the delay time ($\tau/4$) and integration step ($N = \tau/4/tint$). Integration time ($tint$) is established by the phase velocity, source and load dynamics. Details on each of these blocks follows.

III. Inverter Source Model

The source is modeled with a charged electrolytic dc bus capacitor, along with series stray inductance and resistance. The source is passed through a step source switch with a risetime from zero to dc bus voltage that is variable and which represents device rise and fall time. Thus, risetimes for IGBT's (40 ns to 400 ns), BJT's (250 ns to 2 μ s), GTO's (2 μ s to 4 μ s) or any user defined risetime may be modeled.

IV. Transmission Line Model

Modeling cables and transmission lines is a complex problem; the complexity dictated by the accuracy of the simulation. At normal operating carrier or switching frequencies a lumped parameter series R-L model may be sufficient for drive applications. However, the rise time of modern switching devices is now in the sub microsecond range and contain significant high frequency content, therefore requiring a more complex transmission line model for investigations of steep wavefronts on motor overvoltage.

Historically, transmission line modeling has periodically received renewed interest by various industries. The earliest attempts at simulating transmission lines dates to the early 1900s [5,6]. Improvements were made in the models and by the late thirties TNA was developed [7]. These simulators were constructed by connecting discrete components to represent transmission lines - essentially lumped parameter models. With the development of modern computing capabilities, the sixties and seventies spawned investigations into distributed parameter models and analysis techniques. Lossless, distortionless, distortion, and frequency dependent models were developed and applied to power system transients [8-11].

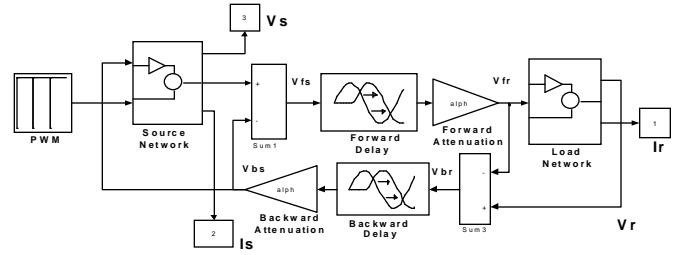


Figure 4a SIMULINK Model for Inverter Drive System.

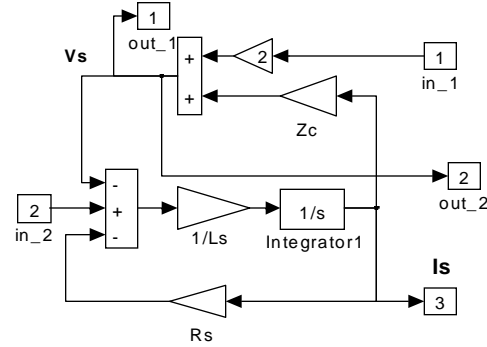


Figure 4b. SIMULINK Model for Source and Leakage Reactance.

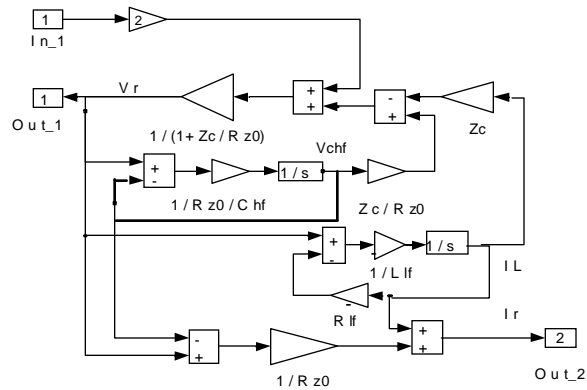


Figure 4c. SIMULINK Model for Machine Load.

Fig. 1 displays the classical incremental transmission line model. The circuit parameters are: series resistance (r) in Ω/m , series inductance (l) in H/m, the shunt conductance (g) in Ω^{-1}/m , and the shunt capacitance (c) in F/m. The complexity of cable and transmission line modeling becomes apparent by examining the forward propagation impulse response for a single conductor line to a unit step $\delta(T)$.

$$h(T, x) = e^{-\xi x} \delta(T) + \frac{\eta}{v} e^{-\xi x} e^{-\xi T} \left[a_0 + a_1 T + a_2 T^2 + a_3 T^3 + \dots \right] u(T) \quad (1)$$

$$\xi = \frac{\left(\frac{r}{l} + \frac{g}{c} \right)}{2} \quad \eta = \frac{\left(\frac{r}{l} - \frac{g}{c} \right)}{2} \quad v \approx \frac{1}{\sqrt{lc}} \approx \frac{c}{\sqrt{\epsilon_r}} \quad T = t - \frac{x}{v}$$

The line parameters determine $a_0 \dots a_n$ [12]. Velocity of propagation (v) is usually less than the speed of light (c) and dependent on conductor spacing and insulation dielectric constant (ϵ_r).

The first term in the forward propagation impulse response represents an impulse which is attenuated and delayed. A line to line voltage pulse, when applied to an uncharged line, will arrive at the motor terminals after a delay of $x\sqrt{lc}$ seconds from $v = \partial x / \partial t$. The attenuation depends on the distance and damping (ξ) of the transmission line. The second term, however, describes the distortion present in the response as the wave travels from the sending end to the receiving end.

Transmission lines are traditionally divided into lossless (r and $g = 0$), low loss ($r \ll \omega l$, $g \ll \omega c$), and distortionless ($r/l = g/c$). Although lossless and distortionless represent unrealistic conditions, the wave equations are easily understood and analyzed. Even though this may not be strictly correct, experience has shown this approximation is acceptable for investigating motor over-voltages. Furthermore, these assumptions are often acceptable because of marginal improvement obtained from more detailed models.

A. Transport Delay

Propagation constant (γ) and characteristic impedance (Z_c) for transmission line cables are functions of the circuit parameters and given by

$$\gamma = \sqrt{(r + j\omega l)(g + j\omega c)} = \alpha + j\beta \quad (2)$$

$$Z_c = \sqrt{\frac{r + j\omega l}{g + j\omega c}} \quad (3)$$

The imaginary part of this expression provides the transport delay of the transmission line, and can become quite complex. Oscillation frequencies vs. cable length (a) for representative cables were presented in Fig. 6 of [13]. Under certain conditions, the relationship between the propagation constant and the oscillation frequency is given by

$$f_o = \frac{\omega}{4\alpha\beta} = \frac{1}{4a\sqrt{lc}} \quad (4)$$

The propagation constant and oscillation frequency are critical parameters for accurate prediction of the damping time and peak terminal voltage when subjected to PWM operation [13,14].

B. Lossy, Lossless and Distortionless Model

A lossless line yields a pure imaginary propagation constant. A distortionless line adds an attenuation factor. More realistic models include the ac skin effect losses, with approximations made depending on the relative magnitudes of the circuit components. Summarizing using reference [15].

1) Lossless line ($r = 0$, $g = 0$): Ideal conditions

This assumption is not used here since it leads to gross inaccuracies during transients (Fig. 3). However, it may be used with some success when filter characteristics dominate over line parameters (Fig. 2).

$$\gamma = j\beta = \omega\sqrt{lc} \quad (5)$$

$$Z_c = r_c + jx_c = \sqrt{\frac{l}{c}} \quad (6)$$

2) Low loss line ($r \ll \omega l$, $g \ll \omega c$): Very high frequencies

This assumption is also not used. It can only be met at high frequency as noted by [15] and evidenced by observing measured cable parameter data vs. frequency of Section VI.

$$\gamma = \alpha + j\beta \cong \frac{1}{2} \left(r\sqrt{\frac{c}{l}} + g\sqrt{\frac{l}{c}} \right) + j\omega\sqrt{lc} \quad (7)$$

$$Z_c = r_c + jx_c \cong \sqrt{\frac{l}{c}} \quad (8)$$

3) Distortionless Line ($r/l = g/c$): Unique condition

The assumption of a distortionless line implies the ratios r/l and g/c are equal although substitution of measured data from section VI shows this unique condition may not occur. However, by assuming a distortionless line ($\eta = 0$), the model is simplified and easily simulated. Experience has shown this approximation is acceptable for investigating motor overvoltages. Section IV-E investigates a $r \neq 0$, $g \approx 0$ condition and shows that pulse distortion is low for large gauge wire and dominated by ac skin effect resistance during the pulse risetime.

$$\gamma = \alpha + j\beta = r\sqrt{\frac{c}{l}} + j\omega\sqrt{lc} \quad (9)$$

$$Z_c = \alpha + j\beta = \sqrt{\frac{l}{c}} \quad (10)$$

C. Selection of Transmission Line Model

The forward propagation impulse response, (1), may now be examined assuming the conditions for a lossless line, low loss line, distortionless line, and a line with distortion. Clearly, the lossless line has an impulse response of a pure delay.

$$\xi = \eta = 0, T = t - x\sqrt{lc} \quad (11)$$

The impulse response for the distortionless line contains an attenuation in addition to the delay.

$$\xi = \frac{\left(\frac{r}{l} + \frac{g}{c} \right)}{2}, \eta = 0, T = t - x\sqrt{lc} \quad (12)$$

For all other conditions, the impulse response consists of a delayed component with attenuation plus a sequence of distortion terms [6,11]. In addition, cable parameters are not independent of frequency; thus, a transmission line model incorporating frequency dependent parameters may be necessary [6,16,17].

The distortionless line assumption of (12) is used in the SIMULINK program. Equation (13) is the pulse attenuation term previously derived in [13] for the case of $g = 0$. It is seen that (13) and the generalized traveling wave equation (1) are identical when substitution of $g = 0$ into (12) along with ξ and v into (1) is done.

$$\frac{e}{e_o} = \epsilon^{-\left(r_{ac}x/2Z_o\right)} = \epsilon^{-\left(r_{ac}vt/2Z_o\right)} = \epsilon^{-\left(r_{ac}/2l\right)t} \quad (13)$$

The simulated transmission line model is based on cable characteristics, which in turn is based on cable geometry, such as cable insulation material and spacing between conductors. Input data is the distributed cable parameters of l , c , r and g that were measured for various cable configurations in Section VI. Parameters were measured as a function of frequency for the case of two wires in parallel and the third as a single wire return.

Transport delay is a function of cable insulation material and spacing between conductors. Equation (1) states wave velocity v is a function of relative dielectric constant ϵ_r . Wires widely separated in air have $\epsilon_r = 1$ and $v = c$, while a bundled cable has a defined insulation material ϵ_r and a lower v . In between the two extremes, there is an "effective ϵ_r " defined by a simple series combination of an air capacitor and insulation capacitor. Fig. 5 shows an "effective ϵ_r " for each material tends toward one when $[x_o/2x_l]$ is > 20 . x_o is the air space distance between insulation edges and x_l is conductor insulation thickness.

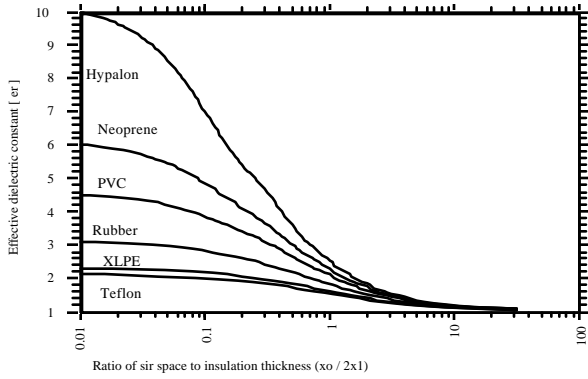


Figure 5. Relative Dielectric Constant (ϵ_r) vs. Insulation Thickness.

With defined l and c input parameters, the cable natural oscillation frequency f_o is accurately determined. Skin and proximity effects on cable resistance as a function of f_o are calculated with reasonable accuracy for most wire gauges using skin effect equation factors of [13] and forward and reverse ξ factors are simulated.

D. Lumped vs. Distributed Model vs. Transport Model

A single PWM pulse of velocity (v) from the drive traverses a transmission line of length (a) four times per oscillation period (τ) due to the fact that the motor end appears as an open circuit $\Gamma_m \sim 1$ while the inverter end appears as a short circuit $\Gamma_i \sim -1$ [13]. Velocity v is defined in (14) for inductance per meter (l) and capacitance per meter (c) uniformly distributed along the length of the line. The number of oscillations in 2π seconds is called the natural or eigen frequency (ω_o) of the distributed line.

$$\tau = \frac{4a}{v} \text{ where } v = \frac{1}{\sqrt{lc}} \quad (14)$$

$$\omega_o(\text{distributed}) = \frac{2\pi}{\tau} = \frac{\pi v}{2a} = \frac{\pi}{2a\sqrt{lc}} = \frac{\pi}{2} \frac{1}{\sqrt{LC}}$$

A single loop lumped parameter model with capacitance (C) concentrated at the open or motor end and inductance (L) concentrated at the short circuit or inverter will have a natural oscillation frequency defined by (15).

$$\omega_o(\text{lumped}) = \frac{1}{\sqrt{LC}} \quad (15)$$

Thus, a distributed line model "eigen" frequency is $\pi/2$ or 1.57x greater than a single lumped L - C model. As an example, consider the 500 ft of #12 AWG wire in [13] that produced a measured 250 kHz line oscillation frequency. The calculated natural eigen frequency for distributed parameters $rdc = 1.65 \Omega / 1000 \text{ ft}$ and $l = 0.55 \mu\text{H} / \text{m}$ and $c = 77 \text{ pF} / \text{m}$ lumped into a single loop matrix in (16) is $1.0008 \text{ e}6$ or $1.0008 \text{ e}6 / 2\pi = 159,282 \text{ cy/sec}$. Thus, measured distributed model ω_o ratio to the calculated lumped model is 1.569.

Single loop matrix

Eigenvalues

$$\begin{bmatrix} \frac{R}{L} & -\frac{1}{L} \\ -\frac{1}{L} & -\frac{1}{L} \\ \frac{1}{C} & 0 \end{bmatrix} \quad \begin{pmatrix} -1.4811 \cdot 10^3 + 1.0008 \cdot 10^6 i \\ -1.4811 \cdot 10^3 - 1.0008 \cdot 10^6 i \end{pmatrix} \quad (16)$$

Errors in modeling the natural frequency result in erroneous peak voltages in the > 2 pu transient mode of PWM double pulse simulation [13,14]. This is due to the fact that trapped reverse voltage during line to line dwell time of Fig. 6 is not accurately determined. Errors in line oscillation frequency also directly affect the skin effect ac resistance

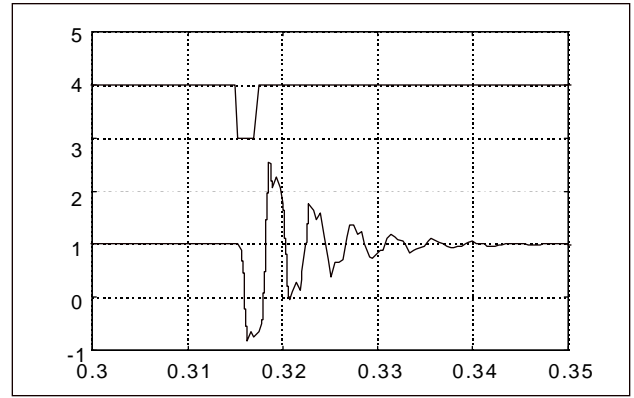


Figure 6. Simulation Results of PWM Double Pulsing using Distributed π Model.

and produce erroneous damping during the dwell time of Fig. 7, resulting in peak voltage errors in the > 2 pu transient mode.

Cable eigen frequencies tend to increase to much higher values as the line cable is broken down into a number of multiple lumped π section models. This implies that time steps must be very small to get accurate results, an effect that was confirmed with distributed π model simulation. Also, as more sections are added, convergence problems appear as well as longer time simulations.

The transport delay model accurately predicts propagation time, oscillation frequency ω_o , determines ac skin effect resistance as a function of ω_o , has no convergence problems and is a relatively fast simulation. Thus, this is the preferred model to determine cable damping effects and transient over-voltages in drive-motor-cable systems.

E. Distortionless Line Assumption

Drive output risetime (t_{rise}) is defined as 10% to 90% of Vdc bus. This section investigated how much the risetime at the motor terminals (also 10% to 90% of Vdc) is additionally sloped for long cable lengths and various wire gauges.

Fig. 8 plot shows that any additional sloping t_{slope} beyond the initial original risetime appears to be a function of wire gauge and cable distance. Smaller gauge wires provide greater t_{slope} with cable distance than larger diameter wires. However, for cables less than 600 ft, there is no large beneficial sloping effect of the steep front drive pulse for conductors greater than #12 AWG. Thus, a low pulse distortion assumption used in the SIMULINK program is justifiable.

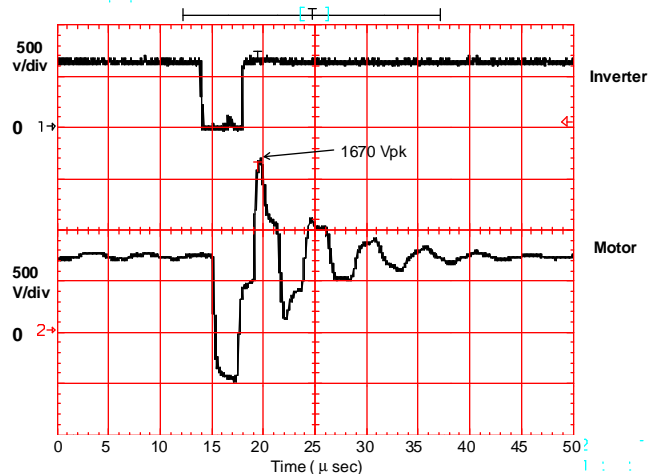


Figure 7. Experimental Data from a PWM Drive to Demonstrate Double Pulsing.

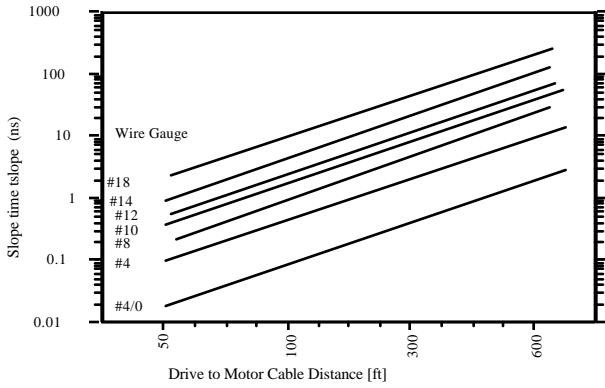


Figure 8. Slope time for Wire Gauges vs. Distance.

V. Motor Model

The adverse effects of steep voltage wavefronts on machine windings have resulted in extensive investigations into motor terminal over-voltages [14, 18-22]. IGBT based PWM voltage source inverters, with very low rise times, subject the receiving end ac induction machines to extreme voltage stress many thousands of times per second. Peak line to line terminal over-voltage (V_{pk}) at the receiving end of an *initially uncharged* transmission line subjected to a *single PWM pulse* with risetime t_r was derived in [23]. Equation (17) applies at cable distances equal to or greater than a critical cable distance l_c , which is the point at which the reflected wave is fully developed for a given pulse risetime [24]. V_{dc} is the drive dc bus voltage and Γ_m is the reflection coefficient ($0 < \Gamma_m < 1$) at the motor. V_{pk} magnitude is highly sensitive to the surge impedance mismatch between motor surge impedance Z_m and cable surge impedance Z_o . V_{pk} magnitude is a possible maximum $2 V_{dc}$ at cable length l_c and decreases to V_{dc} for a short cable at the drive output. Thus, cable length and pulse risetime are the predominant factors in determining V_{pk} in the < 2 pu mode below l_c . The following sections give methodologies to experimentally determine a Z_m magnitude vs. motor hp size, since it is the key ingredient in determining V_{pk} .

$$V_{pk} (@ l_c) = (1 + \Gamma_m) V_{dc} \text{ where } \Gamma_m = \frac{Z_m - Z_o}{Z_m + Z_o} \quad (17)$$

Receiving end V_{pk} magnitude may approach $3 V_{dc}$ for cable lengths $> l_c$ when the transmission line has an *initial condition of trapped charge* due to *multiple PWM pulses*. The interaction between cable transient damping characteristics, motor dynamic surge impedance model and PWM pulse spacing are the predominant factors in determining V_{pk} in the > 2 pu mode above l_c [14]. The last section incorporates the Z_m value seen during the pulse risetime into a simplified high frequency model of the ac induction motor to get accurate system simulations in the > 2 pu reflected voltage mode.

A. Identifying Motor Surge Impedance using Inverter Pulses.

The apparent motor surge impedance (Z_m) observed during the rising edge of the reflected wave front was measured under drive operation using $Z_m = \Delta e / \Delta i_{pk}$. Line to line voltage V_{ac} was measured during the PWM pulse condition that changed phase A,B and C connection from the (+) dc bus to Phase C connection to (-) bus. The value Δe is the transient peak voltage above the dc bus magnitude during t_{rise} and Δi_{pk} is phase C peak transient phase current into the motor. Fig 9 shows how Z_m varies with hp when

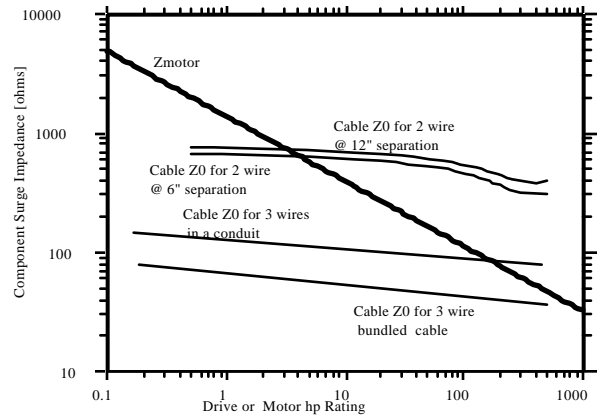


Figure 9. Measured Surge Impedance vs. HP Size.

measured during the pulse risetime. Motor surge impedance is not an absolute value since a 1 hp motor varied between 1,000 to 5,000 ohm surge impedance depending on the motor manufacturer. Thus, rather than an absolute Z_m magnitude vs. hp line, there is probably a Z_m band to investigate for model use. Approximate values of $Z_m = 1,000 \Omega$ for a 1 hp motor and $Z_m = 100 \Omega$ for a 100 hp motor are inferred from Fig. 9.

B. Identifying Motor Surge Impedance with a RLC Analyzer

HP Impedance Analyzer 4284 test leads were connected to motor phase A - phase B in parallel and motor phase C to simulate the surge impedance observed during a reflected wave transient. Impedance and Phase Angle vs. Frequency plots are shown in Fig. 10 for 1 and 100 hp motors.

Motor phase angle approaches a positive maximum near 2 kHz to 3 kHz. This is due to magnetic skin effect in the motor laminations which reduce iron core ac inductance L_{ac} . High frequency eddy currents limit the depth of flux penetration and cause a reduction in iron permeability from μ_i to μ and reduce the apparent L_{ac} . Critical frequency f_{core} defines the frequency at which flux penetration skin depth (δ) is equal to lamination thickness (k) or $\psi = 1$. Above f_{core} eddy current shielding becomes substantial and stator iron core inductance starts to drop. Substitution of resistivity (ρ) and thickness (k) for 12 mil steel in (18) results in a typical motor f_{core} of 3.3 kHz as in Fig. 10 [25].

$$\frac{\mu}{\mu_i} = \frac{L}{L_i} = \frac{1}{\psi} \frac{\sinh \psi + \sin \psi}{\cosh \psi + \cos \psi} \quad (18)$$

$$\psi = \frac{k}{\delta} \text{ and } \delta = \sqrt{\frac{2\rho}{2\pi f_{core} \mu_i \mu_0}}$$

Reduction of iron core inductance continues above f_{core} until values approaching wire self inductance and stator air core leakage inductance's are reached at resonant frequencies (f_r) of 25 kHz for the 1 hp motor and 55 kHz for the 100 hp motor. Historical literature, as well as Finite Element Analysis (FEA) of random wound wires in a slot [26], suggest that flux is contained around the wire periphery with no penetration into the core at high frequencies. Beyond f_r , turn to turn and turn to ground capacitance of the wires in the slot as well as coil to coil capacitance are predominant, such that phase angle now approaches (-90) degrees at high frequencies near 1 MHz.

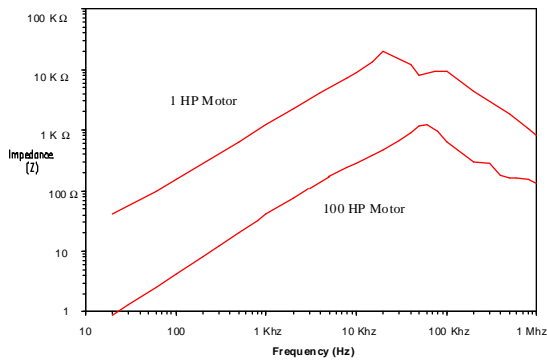


Figure 10a. Motor Impedance vs. Frequency Relationship.

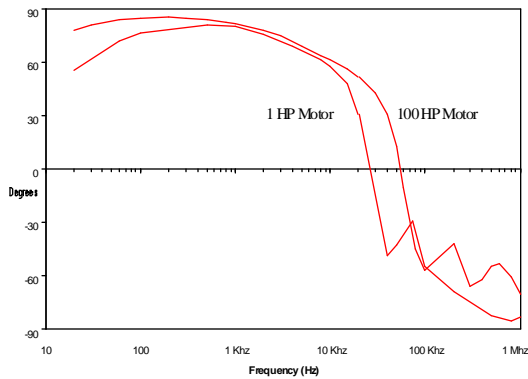


Figure 10b. Motor Phase Angle vs. Frequency Relationship.

Fourier analysis of the PWM pulse defines an equivalent high frequency (f_u) that corresponds to pulse risetime (t_{rise}). Table I calculates f_u for various pulse risetimes using (19). The motor surge impedance that is presented to the arriving PWM pulse risetime is the Fig. 10 impedance magnitude that corresponds to frequency f_u . For a typical IGBT $t_{rise} = 0.2 \mu s$ with $f_u = 1.6 \text{ MHz}$, a 1 hp motor surge impedance is thus $1,000 \Omega$ and a 100 hp motor $Z_m = 100 \Omega$ from Fig. 10. These Z_m values agree with those determined from inverter pulse testing. It is seen from Fig. 10, that motor Z_m will vary with pulse risetime applied.

$$f_u = \frac{1}{\pi t_{rise}} \quad (19)$$

Table I Equivalent Frequencies of Various Pulse Risetimes

t_{rise} [μs]	0.05	0.1	0.2	0.4	1	2
f_u [kHz]	6,366	3,183	1,600	795	318	160

Rather than just obtaining a lumped Z_m value, the next section attempts to incorporate Z_m into a high frequency model of the ac induction motor.

C. High Frequency Models of AC Motors

Numerous investigations into high frequency modeling of ac induction machines were recently reported [26-30]. High frequency motor models may be subdivided into two broad categories depending on the purpose of the analysis. First, models based on FEA propose to examine the machine on a per turn level [26]. FEA models are complex and are primarily for motor design purposes. The second category's purpose is to develop reduced order models, easily

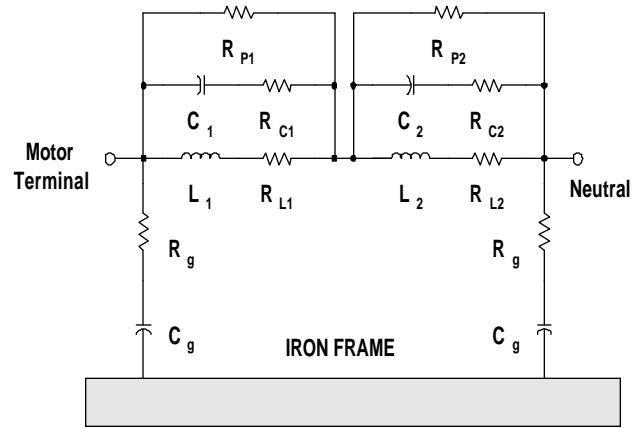


Figure 11 Recently Proposed Motor Model [27].

interfaced to simulation software, resulting in a software package designed to examine application specific problems [14,22].

Recently, a model was proposed based on data obtained from a 1.5 kW machine and is repeated in Fig. 11 [27]. This model is a per coil group model incorporating mutual and leakage inductance terms, inter-turn capacitance, and corresponding loss resistances. In the case presented in [27], the machine consisted of two coil groups per phase in a 380 v Y winding arrangement. As is clear from the figure, this model implies high frequency current conducts from one coil group to the next through the winding conductor. However, tests were conducted on a wound rotor, 5 hp, 4 pole, 230/460 volt, ac induction motor while excited by an IGBT based inverter. Fig. 12 shows the input current (I_s), terminal voltage (V_t), and winding midpoint current (I_{sm}) with a 460 volt connection. Notice the input current and terminal voltage are rich in high frequency content - the dominant frequency approximately 7 MHz. At the midpoint, however, the high frequency was totally absent. This suggests the model of Fig. 11 is inadequate.

Further investigations were conducted with the rotor open circuited in addition to its normal short circuited arrangement. Fig. 13 shows I_s , V_t , and the open circuited rotor voltage (V_{rli}) at 0 rpm and nominal flux current applied to the machine. The carrier frequency was 4 kHz and an IGBT rise time of approximately 100 ns. Notice the induced rotor voltage oscillates at 250 kHz with no indication of the 7 MHz signal present in V_t and I_s . Repeating with the rotor short circuited produces the results of Fig. 14. In this case, the rotor current is monitored. Again no high frequency is present. These results indicate the high frequency is confined to the stator and is only conducted into a portion of the stator winding.

D. Motor Model For Differential Reflected Wave Simulations

From the results above and those reported in [14], a differential or line to line mode motor model for purposes of predicting the peak line to line motor terminal voltage (V_{term}) is set forth in Fig. 15. The significant differences with the model presented in [27] lies with the parasitic capacitance's from line to line (C_{ll}). The topology of the circuit, essentially a resonant tank circuit, provides a relatively simple interface to transmission line models. The parameters are obtainable through system identification procedures and values tabulated for various motor ratings. The capacitor series resistance, R_{z0} , corresponds to the surge impedance of the machine and establishes the reflection coefficient. This resistance differentiates the proposed model from that presented in [28], wherein the line to line capacitance serves to short the stator terminals at high frequency. The remaining parameters may be estimated from frequency data, such as Fig. 10, obtained from tests performed using a LCR meter such as HP's 4284. Table II contains results for 1, 10 and 100 hp motors that corresponds to the load motor model of Fig. 4c. Parameters C_{hf} and R_{z0} determine

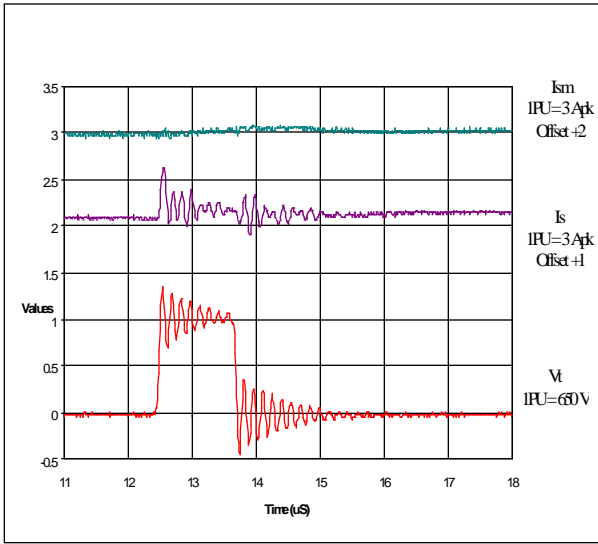


Figure 12 Experimental Data to Demonstrate the High Frequency Relationships.

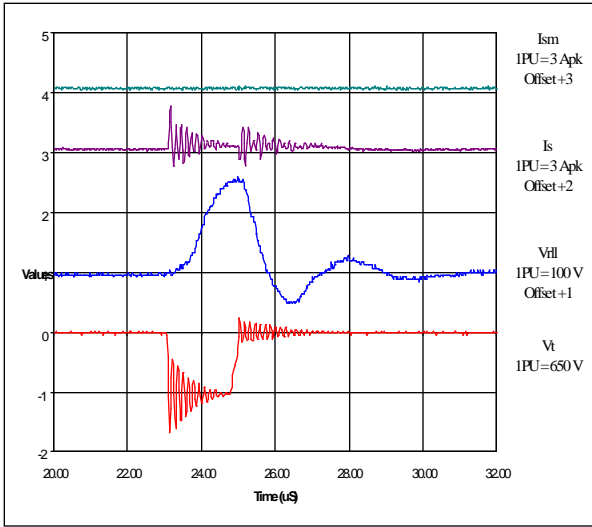


Figure 13. Experimental Data to Demonstrate the Open Circuited Rotor Voltage Characteristics.

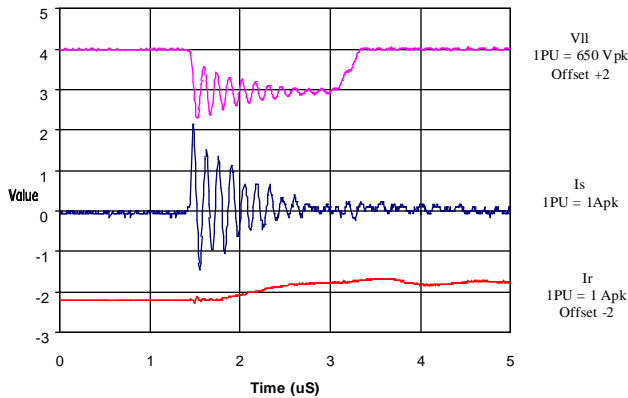


Figure 14. Experimental Data to Demonstrate the Shorted Rotor Current Characteristics.

the high frequency model response while R_{lf} and L_{lf} still allow an accurate model for low frequency modeling.

Table II Motor Model Parameters

	1hp	10 hp	100 hp
R_{z0}	1000 Ω	400 Ω	100 Ω
R_{lf}	25 Ω	1.76 Ω	0.18 Ω
C_{hf}	190 pF	600 pF	6.48 nF
L_{lf}	260 mH	110 mH	4.3 μ H

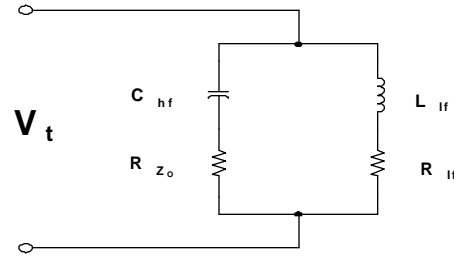


Figure 15. Differential Mode Motor Model.

VI. Cable Parameters vs. Cable Construction

Initially, equations were found to approximate cable inductance and capacitance of simple cable configurations. However, it was found capacitance equations calculated for the same configuration were off by as much as 200 % and correlation to real life constructions was even more difficult. The fact of armor ground totally surrounding the wires and the possibility of multiple grounds in side the cable also complicated inductance formula estimates. Skin and proximity cable resistance for various cables also tended to vary due to the number of strands used and whether the strands are bundled and twisted inside the cable. Thus, to enter accurate cable parameter data into the program the distributed per meter cable parameters for the cable construction techniques in Fig. 16 were measured vs. frequency. Table III values are for two phases in parallel with the third phase used as a return phase using a two wire LCR analyzer. Series inductance ls and series resistance rs per meter were measured vs. frequency with one end of a 1 meter test sample shorted. Capacitance cp and insulation resistance rp from phase 3 to 2 in parallel with phase 1 were measured with the ends of the 1 meter sample open circuited.

VII. Results

A. Measured vs. Simulated for Uncharged Transmission Line

Fig. 17a and 17b shows agreement in the 3τ damping time between measured and simulated results with 500 ft #12 AWG and a 1 hp motor of $Z_m = 1,000 \Omega$. Peak terminal over-voltage 1.8 pu vs. 1.7 pu is also accurately simulated.

B. Effect of Cable Damping Resistance

Motor surge impedance $Z_m = 1,000 \Omega$ of Fig. 17a and 17b was kept constant and wire gauge varied from #12 AWG to # 8 AWG in Fig. 18. Note the unexpected shortened decay time for larger gauge wire. Skin effect rs data for the # 8 AWG (3 wire plus 3 grounds plus armor) is actually greater than for the # 12 AWG cable at the simulated cable oscillation frequency near 100 kHz. Thus, this particular # 8 AWG cable construction provides more damping in Fig. 18 than the smaller wire in Fig. 17b. This example highlights the need to obtain accurate measured cable data, since it is difficult to obtain cable distributed parameter changes with frequency by simple equations for all complex cable configurations.

C. Effect of Load Surge Impedance - Variation With Motor Hp

Fig. 18 and Fig. 19 compares the effect when the # 8 AWG cable is held fixed but a 1 hp motor of surge impedance = 1,000 Ω and its Section V load parameters are changed to a 100 hp motor of surge impedance = 100 Ω and it's respective load parameters.

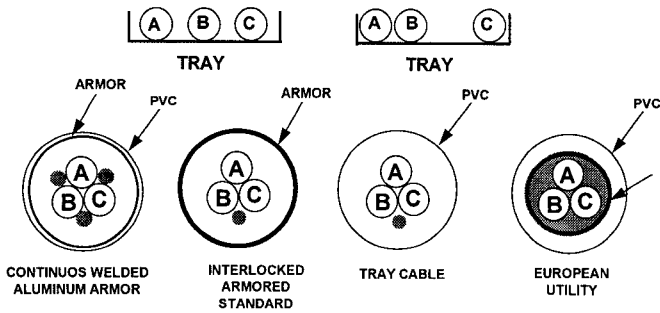


Figure 16 Motor Cable Construction Types

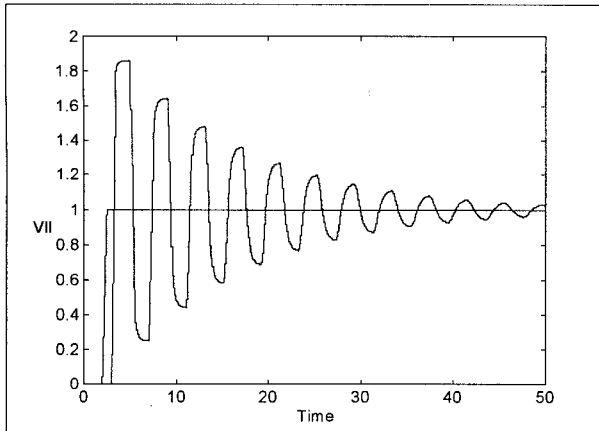


Figure 17a. Simulation of 1 hp Machine with 500 ft of #12 Cable

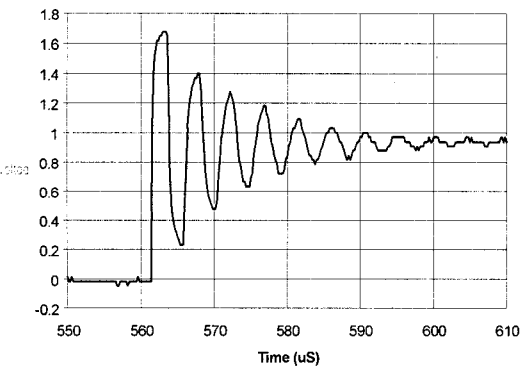


Fig. 17b Experimental Data from 1 hp motor with 500ft of #12 AWG

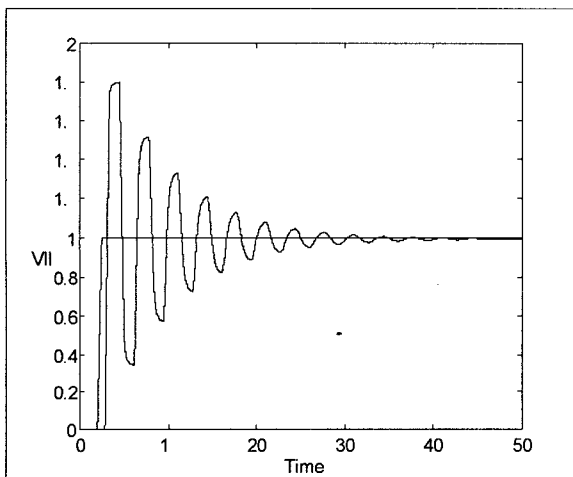


Fig. 18 Simulation of 1 hp Machine with 500 ft of #8 AWG cable

D. Effect of Distributed Vs. Transport Delay System Model

Fig. 7 demonstrates measured > 2 pu transient motor voltage for a PWM double pulse condition [14]. Fig. 6 shows simulation results when using a 5 section distributed π model for the same condition. Fig. 20 results are for the proposed transport delay model. Note the backside porch slopes and general slope correlation between transport delay simulation in Fig. 20 and experimental data of Fig. 7, which is not present in the distributed π model of Fig. 6.

E. Other Effects

The effect of termination network and drive output filters as for low and high hp drive systems are easily analyzed by adding additional SIMULINK blocks.

VIII. Conclusion

This paper proposed a reflected wave drive - cable - motor system model that is simple, computationally fast, reasonably accurate and allows wide variation of system parameters. Physics and facts on distortionless line model assumptions were given. The effect of distributed vs. transport delay type models on modeling accuracy was discussed. To establish correct system models, the paper investigated high frequency characteristic data on both motors and cable parameters that is generally not found in literature. Motor transient voltage results were simulated and compared to experimental waveforms as a function of load hp, cable construction, wire gauge selected, and other reflected wave filter options.

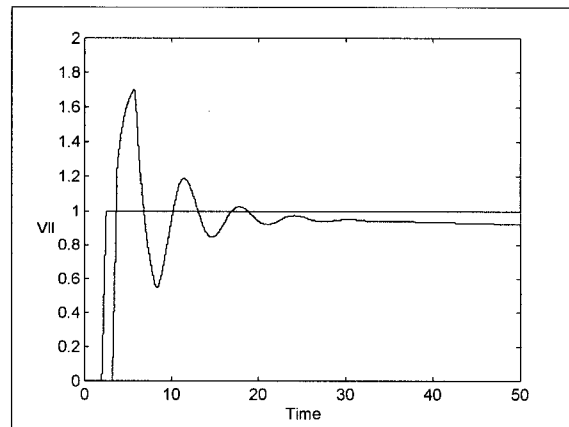


Figure 19 Simulation of 100 hp Machine with 500 ft #8 AWG Cable

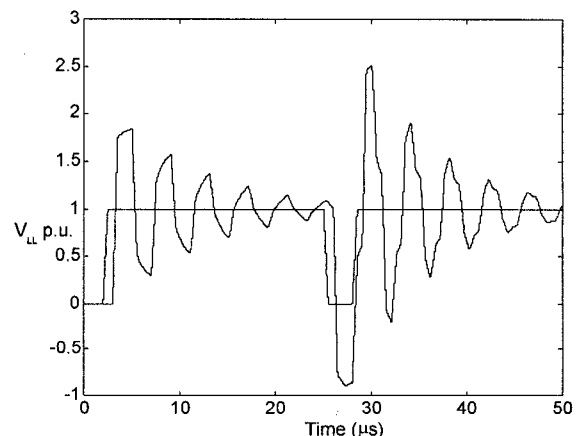


Figure 20 Simulation Results of PWM Double Pulsing with a Modified Transmission Model using Transport Delay Process

Table III Measured Cable Parameters per meter for Various Cable Construction of Fig. 16

350 MCM 3 wire plus ground PVC Armor Cable							#4 awg 3 wire plus ground PVC Armor Cable					#8 awg 3 wire plus 3 gnds XLPE armor Cable						
fo [Hz]	ls [uh]	rs [Ω]	cp [pf]	rp [Ω]	zo	rac / rdc	ls [uh]	rs [Ω]	cp [pf]	rp [Ω]	zo	rac / rdc	ls [uh]	rs [Ω]	cp [pf]	rp [Ω]	zo	rac / rdc
100	0.42	0.0008	338	-	35	1.0	0.55	0.0006	128	-	65	1.5	0.86	0.0067	98	-	93	1.02
1k	0.36	0.0028	257	8.7M	37	3.5	0.45	0.0011	121	19M	61	2.8	0.82	0.0072	98	-	91	1.09
10k	0.34	0.0071	216	271K	40	8.9	0.37	0.0027	109	2M	58	7	0.66	0.0124	98	-	82	1.82
100k	0.34	0.0127	211	137K	40	16	0.35	0.0064	98	265k	59	16	0.55	0.0381	98	15M	75	5.77
1M	0.33	0.0178	204	24K	40	22	0.52	0.0419	84	57k	78	104	0.51	0.1296	80	-	80	20

#2 awg 3 wire Hypalon triangle bundle on ground plane							#2 awg 3 Hypalon wire separated by 6 inch					#2 awg 3 wire + gnd SO Tray Cable						
fo [Hz]	ls [uh]	rs [Ω]	cp [pf]	rp [Ω]	zo	rac / rdc	ls [uh]	rs [Ω]	cp [pf]	rp [Ω]	zo	rac / rdc	ls [uh]	rs [Ω]	cp [pf]	rp [Ω]	zo	rac / rdc
100	0.66	0.0006	52	-	112	1.0	1.6	0.0003	1.4	-	1068	1.0	0.7	0.0009	84	-	91	1.0
1k	0.51	0.0007	55	-	96	1.17	1.48	0.0005	3.2	-	679	1.7	0.54	0.0010	78	50M	83	1.11
10k	0.48	0.0024	54	22M	94	4.0	1.44	0.0019	3	-	700	6.3	0.51	0.0031	75	8M	82	3.4
100k	0.44	0.0137	53	3M	91	22.8	1.41	0.0129	2.86	28M	702	43	0.45	0.0236	73	1M	78	27
1M	0.6	0.0705	52	414K	107	117	1.57	0.0685	2.8	9M	750	228	0.41	0.0948	70	102K	77	105

#10 awg PVC 3 wire plus gnd plus braid shield Cable							#12 awg 3 wire + gnd SO Tray Cable Cable					#16 awg 3 wire + gnd SO Tray Cable						
fo [Hz]	ls [uh]	rs [Ω]	cp [pf]	rp [Ω]	zo	rac / rdc	ls [uh]	rs [Ω]	cp [pf]	rp [Ω]	zo	rac / rdc	ls [uh]	rs [Ω]	cp [pf]	rp [Ω]	zo	rac / rdc
100	0.95	0.0101	265	66M	60	1.0	0.7	0.0103	47	-	128	1.02	0.80	0.0238	43	-	136	1.0
1k	0.77	0.0102	235	7M	57	1.01	0.86	0.0106	47	-	136	1.03	0.80	0.0238	43	7-	36	1.0
10k	0.74	0.0152	206	876k	59	1.5	0.84	0.0117	47	38M	135	1.14	0.80	0.0244	43	68M	36	1.03
100k	0.54	0.0768	182	123k	55	7.6	0.80	0.0267	45	2M	133	2.59	0.77	0.0409	42	5M	35	1.73
1M	0.61	0.3099	80	30k	87	31	0.76	0.1764	44	161K	133	17	0.73	0.2070	41	298K	133	8.7

References

[1] H. Dommel, *Electro-magnetics Transients Program & Theory Manual* Bonneville Power Administration, Portland, Ore

[2] Is-SPICE, Intusoft, Inc.

[3] SIMULINK with MATLAB, The MathWorks, Inc.

[4] Chee-Mun Ong, *Dynamic Simulation of Electric Machinery: Using Matlab/Simulink*, Prentice Hall PTR, Upper Saddle River, NJ

[5] J. H. Cunningham, "Design, Construction, and Test of an Artificial Transmission Line," *Transactions of AIEE*, Vol. 30, Part 1, 1911, pp. 245-256.

[6] J. R. Carson, "Wave Propagation in Overhead Wires with Ground Return," *Bell Systems Technical Journal*, Vol. 5, 1926, pp. 539-554.

[7] H. A. Peterson, "An Electric Circuit Transient Analyzer," *General Electric Review*, September 1939, pp. 394-400.

[8] C. H. Thomas, "Transport-Time Delay Simulation for Transmission Line Representation," *IEEE Trans. on Computers*, Vol. C-17, March 1968, pp. 205-214.

[9] G. L. Wilson and J. G. Kassakian, "Effects of Zero Sequence Modeling and Transposition on Switching Surge Overvoltages," *IEEE Trans. Power Apparatus and Systems*, Vol. 93, May/June 1974, pp. 870-877.

[10] P. C. Krause and K. Carlsen, "Analysis and Hybrid Computer Simulation of Multiconductor Transmission Systems," *IEEE Trans. Power Apparatus and Systems*, Vol. 91, March/April 1972, pp. 465-477.

[11] S. J. Balsler, "Distributed Parameter Representation for Low Frequency Transients on Untransposed Transmission Lines," *IEEE PES Summer Meeting*, San Francisco, CA, July 20-25, 1975.

[12] S. J. Balsler, "Distributed Parameter Models for the Simulation of Power Transmission Lines During Low Frequency Transients," Ph.D. Thesis, Purdue University, West Lafayette, IN, December 1974.

[13] G. Skibinski, R. J. Kerkman, D. Leggate, "Cable Characteristics and Their Influence on Motor Over-Voltages," *IEEE APEC Conference Proceedings*, Atlanta, GA, Feb. 23-27, 1997, pp. 114-121.

[14] R. Kerkman, D. Leggate, G. Skibinski, "Interaction of Drive Modulation & Cable Parameters on AC Motor Transients," *IEEE IAS Conference Record*, San Diego, CA, Oct. 6-10, 1996, pp. 722-731.

[15] D. Cheng, *Field and Wave Electromagnetics*, Addison Wesley, 1989

[16] D. P. Carroll and F. Nozari, "An Efficient Computer Method for Simulating Transients on Transmission Lines with Frequency Dependent Parameters," *IEEE Transaction Power Apparatus and Systems*, Vol. 94, pp. 1167-1176, July/Aug, 1975

[17] D. M. Triesenberg, "Analysis and Simulation of Power Transmission Lines by Frequency Response", Ph.D Thesis, Purdue Univ. West Lafayette IN, May 1975

[18] P. Van Paucke, R. Belmans, W. Geysen, and E. Ternier, "Overvoltages in Inverter Fed Induction Machines Using High Frequency Power Electronic Components," *IEEE APEC Conference Proceeding 1994*, pp. 536-541.

[19] T. Takahashi, M. Termeyer, T. Lowery, and H. Tsai, "Motor Lead Length Issues for IGBT drives," *IEEE Pulp and Paper Conference Proceedings*, 1995, pp. 21-27.

[20] C. J. Melhorn and L. Tang, "Transient Effects of PWM ASDs on Standard Squirrel Cage Induction Motors," *IEEE IAS Conference Proceedings*, Orlando, FL, Oct. 8-12, 1995, pp. 2689-2695.

[21] B. Kawkabani, J.J. Simond, and F. Kehtari, "Voltage Peaks of Low Voltage Motors Due to PWM Inverter Supply," *EPE Conference Proceedings 1995*, Sevilla, pp. 465-469.

[22] A. von Jouanne, P. Enjeti, and W. Gray, "The Effect of Long Motor Leads on PWM Inverter Fed AC Motor Drive Systems," *IEEE APEC Conference Proceedings*, Dallas, TX, March 6-9, 1995, pp. 592-597.

[23] G. Skibinski, "Design Methodology of a Cable Terminator to Reduce Reflected Voltage on AC Motors," *IEEE IAS Conference Record*, San Diego, CA, Oct. 6-10, 1996, pp. 153-161.

[24] L. Saunders, S. Evon, D. Kempke, G. Skibinski, "IGBT Drive Technology Demands New Motor and Cable Considerations", *IEEE IAS Petroleum and Chemical Industry Conference*, Sept 23-27, 1996, pp.75-84.

[25] G. Skibinski, "Design and Implementation of a Passive Clamp Resonant Link Inverter for High Power Applications," Ph.D. Thesis, Univ Wisconsin-Madison, 1992

[26] G. Suresh, Hamid A. Toliyat, Dudi A. Rendussara, and Prasad N. Enjeti, "Predicting the Transient Effects of PWM Voltage Waveform on the Stator Windings of Random Wound Induction Motors," *IEEE APEC Conference Proceedings*, Atlanta, GA, Feb 23-27, 1997, pp. 135-141.

[27] G. Grandi, D. Casadei, A. Massarini, "High Frequency Lumped Parameter Model for AC Motor Windings," *EPE'97*, pp. 2.578-2.583.

[28] A. Consoli, G. Oriti, A. Testa, and A. L. Julian, "Induction Motor Modeling for Common Mode and Differential Mode Emission Evaluation," *IEEE IAS Conference*, San Diego, CA, Oct 6-10, 1996, pp. 595-599.

[29] David B. Hyypio, "Effects of Risetime and Cable Length on Motor Insulation Degradation Resulting from Operation on PWM Voltage Source Inverters," *IEEE International Electric Machines and Drives Conference*, IEMDC Record, May 1997, pp. TCS-2.1-TCS-2.3.

[30] D. Hyypio, "Simulation of Cable and Winding Response to Steep Fronted Voltage Waves", *IEEE IAS Conference Proceedings*, Orlando, FL, Oct. 8-12, 1995, pp. 800-806.